RESEARCH PAPER

Decoupling the Contribution of Surface Energy and Surface Area on the Cohesion of Pharmaceutical Powders

Umang V. Shah • Dolapo Olusanmi • Ajit S. Narang • Munir A. Hussain • Michael J. Tobyn • Steve J. Hinder • Jerry Y. Y. Heng

ABSTRACT

Purpose Surface area and surface energy of pharmaceutical powders are affected by milling and may influence formulation, performance and handling. This study aims to decouple the contribution of surface area and surface energy, and to quantify each of these factors, on cohesion.

Methods Mefenamic acid was processed by cryogenic milling. Surface energy heterogeneity was determined using a Surface Energy Analyser (SEA) and cohesion measured using a uniaxial compression test. To decouple the surface area and surface energy contributions, milled mefenamic acid was "normalised" by silanisation with methyl groups, confirmed using X-ray Photo-electron Spectroscopy.

Results Both dispersive and acid–base surface energies were found to increase with increasing milling time. Cohesion was also found to increase with increasing milling time. Silanised mefenamic acid possessed a homogenous surface with a surface energy of 33.1 ± 1.4 mJ/m^2, for all milled samples. The cohesion for silanised mefenamic acid was greatly reduced, and the difference in the cohesion can be attributed solely to the increase in surface area. For mefenamic acid, the contribution from surface energy and surface area on cohesion was quantified to be 57% and 43%, respectively.

Conclusions Here, we report an approach for decoupling and quantifying the contribution from surface area and surface energy on powder cohesion.

ABBREVIATIONS

BET	Brunauer Emmett, Teller model for calculating surface area from gas adsorption isotherms
iGC	Inverse gas chromatography
RH	Relative humidity
SEA	Surface area analyser
SEM	Scanning electron microscopy
vOCG	van Oss Chaudhury, Good method for calculation of acid–base surface energy
XPS	X-ray photoelectron spectroscopy

INTRODUCTION

Cohesion of powders is reported to be dependent on intrinsic properties (*e.g.*, surface functional end groups, surface energy, elastic module and plasticity) (1,2) and particle properties (*e.g.*, particle size, size distributions, shape and surface roughness) (3–7). Particle properties also depend on the powder processing conditions, *e.g.*, type of processing operation, processing temperature, processing and storage RH (8–10). Out of the

U. V. Shah • J. Y. Y. Heng (✉)
Surfaces and Particle Engineering Laboratory (SPEL), Department of Chemical Engineering, Imperial College London, South Kensington Campus London SW7 2AZ, UK
e-mail: jerry.heng@imperial.ac.uk
URL: http://www.imperial.ac.uk/spel

D. Olusanmi • A. S. Narang • M. A. Hussain
Bristol-Myers Squibb Pharmaceuticals, 1 Squibb Drive New Brunswick NJ 08903, United States of America

M. J. Tobyn
Bristol-Myers Squibb Pharmaceuticals, Reeds Lane, Moreton Wirral CH46 1QW, UK

S. J. Hinder
The Surface Analysis Laboratory, Faculty of Engineering & Physical Sciences, University of Surrey, Guildford Surrey GU2 7XH, UK

listed parameters, current literature extensively report on the effect of surface area/particle size and particle shape on cohesion of powders (1,4,5,7,11). Farley and Valentin reported an empirical correlation between cohesion of powders and volume/surface mean particle diameter for inorganic materials. Cohesion was found to increase with decreasing particle size and increasing surface area (12). Since then, many authors have evaluated the effect of particle size on cohesion and powder flow properties for pharmaceutical powders. The basic assumption for most of these studies is that, particles possess isotropic surface energetics and so contribution from surface energy or particle shape was not taken into account.

Heng *et al.* investigated anisotropic surface properties of various pharmaceutical materials. Facet-specific surface energy of a range of crystalline active pharmaceutical ingredients and excipients was correlated to the facet specific functional end groups (13–16). Milling of pharmaceutical materials is one of the most common top-down approaches to achieve a target particle size for active pharmaceutical ingredients. Different particle size reduction routes may result in changes in particle surface properties. Milling of paracetamol resulted in an increase in the dispersive component of the surface energy, and was attributed to the breakage of particles along the weakest attachment energy planes thus exposing high energy facets (17). On the other hand, Ho *et al.* reported that upon milling dispersive component of surface energy of milled *D*-mannitol particles was found to decrease with decreasing particle size. The decreasing trend in dispersive component of surface energy was explained by needle shaped crystals breaking through the geometrically weakest plane exposing hydrophilic crystal facets which have lower dispersive component of surface energy (18). Thielmann *et al.* investigated the surface energetics of untreated, milled and re-crystallised lactose, using infinite and finite dilution inverse gas chromatography. They reported an upward shift in the energy distributions (dispersive as well as specific surface energy components) of milled materials compared to untreated or recrystallised lactose. Increase in the dispersive surface energy was attributed to the amorphous content (19). Das and Stewart have employed finite dilution inverse gas chromatography to observe effect of processing on surface energy of pharmaceutical materials. For indomethacin, dispersive surface energy was found to increase after micronisation, whereas acid–base surface energy was observed to decrease (20). These studies suggest that milling can result in powders with heterogeneous surface energetics, which can be due to the generation of new surfaces exposing different crystal facets varying in facet specific surface energy and/or due to the generation of amorphous content, as a result of processing route and parameters.

Considering the impact of processing on powder surface energy heterogeneity and the anisotropicity in surface property of organic crystalline material, it is essential to take into account contribution from surface energy in addition to surface area and particle shape on cohesion of pharmaceutical powders. This study aims to decouple the contribution from surface area and surface energy on the cohesion of milled pharmaceutical materials.

The effect of milling time on the surface energetics and surface area was studied for mefenamic acid and cohesion was measured for cryogenically milled material with different milling cycles ($n = 1, 3, …, 12$). Cohesion obtained for milled mefenamic acid can be attributed to the combined effect of surface energy and surface area. Surfaces of milled mefenamic acid were silanised to obtain homogenous surface energetics. Post silanisation, cohesion of milled mefenamic acid was attributed to surface area contribution only.

MATERIALS AND METHODS

Materials

Mefenamic acid (2-(2, 3-dimethylphenyl) aminobenzoic acid) (99.0%, Sigma Aldrich, Dorset, UK), methanol (>99.5%, VWR BDH Prolabo, Lutterworth, UK), cyclohexane (>99.0%, VWR BDH Prolabo, Lutterworth, UK) and dichlorodimethylsilane (>99.5%, Sigma Aldrich, Dorset, UK) were used as received.

Methods

Bulk Crystallisation of Mefenamic Acid

Mefenamic acid crystals used for this study were crystallised from a supersaturated solution of mefenamic acid in methanol, prepared at 50°C. The saturated solution of mefenamic acid at 50°C was then cooled to 4°C, in a single step cooling profile. The mefenamic acid crystals were collected after 24 h and filtered using general-purpose laboratory filter paper (Whatman, UK) and dried under ambient conditions for 24 h. Dried crystals were stored in a glass container at ambient conditions and used for further characterisation or processing.

Cryogenic Milling of Mefenamic Acid Crystals

A Retsch Cryo Mill (Retsch Technology GmbH, Haan, Germany) was used for cryogenic milling of mefenamic crystals. 1 g of recrystallised mefenamic acid was charged in a 50 mL grinding jar containing one grinding ball of 25 mm diameter. In a typical set up, the grinding jar is constantly cooled during the pre-cooling, milling and intermediate cooling steps with liquid nitrogen. In the pre-cooling step, the mill was cooled down to the temperature of −70°C using a liquid nitrogen flow through the mill jacket. Milling was performed at a vibrational frequency of 25 Hz for 10 s. Intermediate cooling between two consecutive milling cycles was performed at a

vibrational frequency of 5 Hz for 40 s. Each milling cycle is defined as the milling step and the intermediate cooling step. The effect of milling time on particle size reduction and surface energy was studied by varying the number of milling cycles ($n=1, 3, …, 12$). Post milling, samples were collected and stored in the glass vials for further characterisation and processing.

Silanisation of Milled Mefenamic Acid

Recrystallised mefenamic acid crystals and milled mefenamic acid powders were silanised using a protocol reported in the literature [21]. For milled mefenamic acid, powders were silanised after milling. In a typical process, 500 mg of mefenamic acid powder was added to a 50 mL 5% (v/v) solution of dichlorodimethylsilane in cyclohexane. The mixture was refluxed at 80°C for 24 h. Then, the reaction mixture is allowed to cool down to room temperature and filtered using general-purpose laboratory filter paper (Whatman, UK) followed by drying in a vacuum oven at 80°C for 4 h. Post silanisation, the silanised mefenamic acid powders were stored in a glass vial at ambient conditions.

Surface Energy Analysis

Surface Energy Analyser (SEA, Surface Measurement Systems Ltd., London, UK) was used for surface energy heterogeneity characterisation. Mefenamic acid powders were packed in pre-silanised iGC columns (4 mm (internal diameter)×300 mm (height)) (Surface Measurement Systems Ltd., London, UK). The powder bed was contained with silanised glass wool at both ends to avoid powder bed movement. Approximately 300 mg of processed mefenamic acid material was packed into each column. The columns were conditioned using the SEA equipment for 2 h at 30°C with helium purge at 10 sccm (standard cubic centimeters per minute). Following the pre-treatment, pulse injection measurements were performed at 30°C. Methane was used to determine the column dead time. Helium at a flow rate of 10 sccm was used as a carrier gas for all injections on the columns packed with milled mefenamic acid. For silanised milled mefenamic acid samples, a helium flow rate of 3 sccm was used. A series of dispersive *n*-alkane probes (hexane, heptane, octane, nonane and decane) at a range of concentrations was injected in order to achieve target surface coverages (n/n_m) ranging from 0.7 to 10%. Net retention volumes were calculated *via* a peak maximum analysis using the commonly applied Schultz method [22]. Monopolar probes (dichloromethane and ethyl acetate) were injected at the same concentrations to determine non-dispersive interactions. The surface energy due to the non-dispersive interactions was calculated using the vOCG method reported in the literature [23,24]. Surface energy (dispersive and non-dispersive) as a function of surface coverage was

calculated using the Cirrus Plus - SEA data analysis software (Surface Measurement Systems Ltd., London, UK).

Dispersive and acid–base surface energy calculations using iGC measurements are discussed widely in the literature. Fowkes suggested that the surface energy can be expressed as a summation of components, and a geometric mean for the dispersive component interaction [25]. The non-dispersive interaction can be determined by semi-empirical models, such as those proposed by Owens-Wendt [26]. More recently, specific interactions are determined by Lewis acid–base interactions as proposed by van Oss *et al.* [23]. An excellent review of these theories can be found in elsewhere [27].

The dispersive component of the surface energy, using inverse gas chromatography, is typically determined by employing either, Schultz or Doris and Gray approach [22,28]. Both the methods are widely accepted, reported to give similar results [29]. Acid–base components are determined using monopolar acid–base probes, as detailed by Das *et al.* [24].

For polar probes, van Oss *et al.* used water with $\gamma^+ : \gamma^-$ equal to unity [23], resulting in a "basicity catastrophe" phenomena. Della Volpe and Siboni proposed a different ratio suggesting water as acidic rather than amphoteric [30]. Despite differing in absolute values, the acidity/basicity order is similar for both approaches [31]. For IGC, the γ^+ or γ^- values for the monopolar probes requires further validation, and the acid–base surface energy values for the solid surface only offers a description of the relative acid–base nature [27,32]. Principles of the techniques and a review of current literature including theory, can be found elsewhere [32].

Surface Area Analysis

Approximately 300 mg of milled mefenamic acid/silanised milled mefenamic acid were conditioned under a helium purge at 40°C for at least 12 h. Post-conditioning, the sample mass was measured and used for surface area measurements. A fully automated Micromeritics Tristar 3,000 (Micromeritics Instruments Corporation, Norcross, USA) system was used for the measurement of nitrogen isotherms at −195.8°C. The surface area was calculated using the BET model based on the linear region of the nitrogen adsorption isotherm (from $p/p^o=0.05$ to 0.3) using the Micromeritics Analysis Software (Micromeritics Instruments Corporation, Norcross, USA).

Particle Size and Shape Analysis

The Morphologi G3s particle characterisation system (Malvern Instruments Ltd., Malvern, UK) equipped with a dry powder dispersion unit was used for particle shape and size analysis. Milled mefenamic acid particles were dispersed in octane and a dilute suspension was dispersed on glass coverslips. Octane was allowed to evaporate at ambient

conditions. Particle imaging was conducted using 20× lenses with vertical *z*-stacking enabled, to obtain information of the three dimensionality of the sample. The raw data was filtered using the Morphologi analysis software (version 8.0, Malvern Instruments Ltd., Malvern, UK) to remove partially imaged or overlapping particles on a sample by sample basis using a combination of convexity, solidity and particle width filters. The morphological filters used in this study and their applications are described in detail elsewhere by Gamble *et al.* (33).

X-ray Photoelectron Spectroscopy Analysis

XPS spectra were obtained for silanised and unsilanised cryogenically milled mefenamic acid samples using a ThermoFisher Scientific Theta Probe X-ray Photoelectron Spectrometer (Thermo VG Scientific Inc., East Grinstead, U.K.). In this study, a twin anode AlKα X-ray source with an energy of $hv = 1486.6$ eV was used at 15 kV×20 mA (300 W). All survey spectra were collected at pass energy of 100 eV, whereas all high resolution spectra were collected at a pass energy of 20 eV. After removal of the non-linear (Shirley) background, high resolution spectra were used for the quantification of the functional end groups present on the surface. The peak fitting function used is a Lorentzian–Gaussian (30% L/G) mix product function. The high resolution data was fitted using the Thermo Avantage software (version 5.904, ThermoFisher Scientific Inc., East Grinstead, U. K.).

Polymorph Identification

A PANalytical X'Pert Pro MPD (PANalytical B.V., Almelo, the Netherlands) powder X-ray diffractometer was used for collecting X-ray diffraction spectra for silanised and unsilanised mefenamic acid. All diffraction spectra were obtained using CuKα radiation (1.541 Å) with a Nickel filter, a fixed 10 mm mask, a soller slit of 0.04 rad, an antiscatter slit of 1/2° and a divergence slit of 1/4°. Measurements were obtained over the angular range from 5-60º 2θ at the 0.08º 2θ step size and time per step of 35 s.

Scanning Electron Microscopy

A TM-1000 (Hitachi High-Technologies Europe GmbH, Krefeld, Germany) table top scanning electron microscope was used for acquiring SEM images. Samples were mounted on the carbon adhesive discs (10 mm), gold coated using a sputter coater at 50 mA for 4 min. SEM images were acquired at an acceleration voltage of 15 kV.

Differential Scanning Calorimetry

Thermograms of the samples were obtained using a TA Q2000 differential scanning calorimeter (TA Instruments, New Castle, DE, USA), connected to the Platinum software. 5–10 mg of samples were loaded in the aluminium pans, which were hermitically sealed using the TA supplied crimping tool. Thermal behaviours of the samples were studied under nitrogen purge at a heating rate of 10°C min^{-1}, over a temperature range from 20°C to 250°C. Thermograms were analysed using the Universal Analysis software supplied as a part of Advantage Software v5.5.3 (TA Instruments, New Castle, DE, USA).

Uniaxial Compression Test

Powder cohesion is the tendency of like particles adhering to each other. Powder cohesion was measured using the uniaxial compression test. Cylindrical compacts were prepared using a 5 mm evacuable pellet die (Specac Ltd., Slough, UK) at a minimum of three different consolidation loads using the SMS texture analyser TA.XT2i (Stable Micro Systems Ltd., Godalming, UK). The compacts varied in height depending on the bulk density of the material. However, an L/D ratio of at least 2:1 was maintained for the compacts. Unconfined yield stresses of the compacts were measured using a 36 mm diameter cylindrical aluminium probe and a 5 kg load cell operated in a displacement compression modes with a test speed of 0.02 mms^{-1}. Each yield stress measurement was repeated three times and was plotted as a function of consolidation stress (*X*-axis). Cohesion and the angle of friction are determined from the intercept and gradient, respectively, of this plot of yield stress *versus* consolidation stress. Details of the theoretical principles of this test method can be found elsewhere (34,35).

RESULTS AND DISCUSSION

Effect of Processing of Mefenamic Acid on Cohesion

To investigate the effect of milling on the surface energy, mefenamic acid crystals obtained from supersaturated solution of mefenamic acid in methanol were milled at cryogenic conditions. The milling time was increased by increasing the milling cycles. Each milling cycle contains two steps, milling and intermediate cooling. Figure 1 shows the dispersive surface energy (γ^d) at three different fractional surface coverages (isosteres) from the surface energy heterogeneity profile of mefenamic acid crystals milled for different numbers of cycles.

Fig. 1 Dispersive surface energy at three different fractional surface coverages (n/n_m) for mefenamic acid crystals milled at cryogenic temperature.
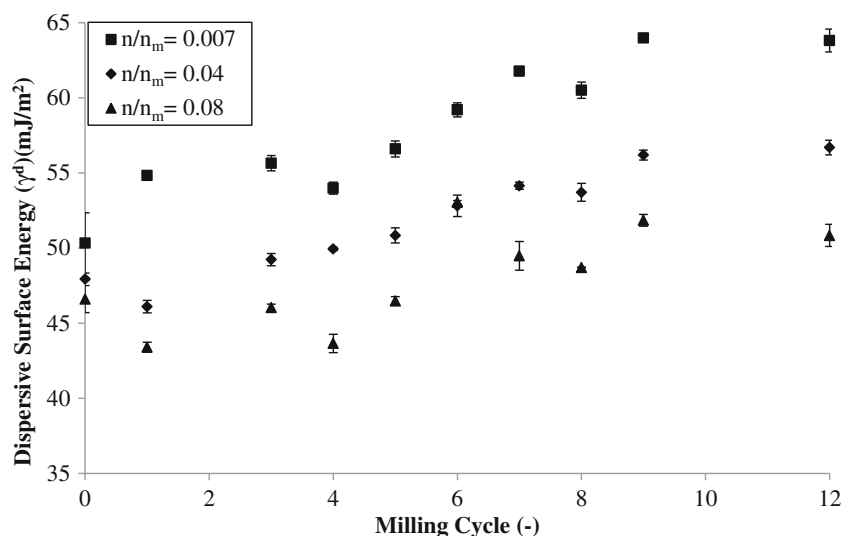

Figure 1 suggests that the surface energy heterogeneity increases post milling, *i.e.* γ^d for mefenamic acid recrystallised from methanol, before milling, ranges from 50.3 mJ/m^2 to 46.6 mJ/m^2 with varying fractional surface coverage (n/n_m) from 0.7 to 10% and after one milling cycle γ^d for mefenamic acid powder varies from 54.6 mJ/m^2 to 43.3 mJ/m^2.

Surface energy heterogeneity profiles (both γ^d and γ^{AB}) were found to be in ascending order with increasing milling cycles (Figs. 1 and 2). Typical variation in the values of γ^d and γ^{AB} measured using inverse gas chromatography is ~±1 mJ/m^2. It is widely reported in the literature that significant amount of energy involved with the milling operation can result in various degree of disorder in the form of crystals defects to the generation of amorphous regions (36–38). Amorphous solid is a solid that lacks long-range molecular order observed in the crystals and hence, any surface disordered caused by the high intensity milling was treated as an amorphous phase. The amorphous content generated during milling can be a function of many different factors including size distribution of un-

milled material, milling temperature, time and intensity (39). While this study involves cryogenic milling, which is reported to prevent the generation of amorphous content during milling, it is argued that the intensity of milling and prolonged milling times allow the formation of amorphous content (40). Elamin *et al.* reported that upon milling, the first evidence of the amorphous content can be found on the surface of crystalline particle and further increases in milling intensity or milling time may then result in generation of bulk amorphous content (38, 41). Considering the experimental evidence provided by Elamin *et al.* (41), it is postulated that the low amount of amorphous content generated in the current study may be limited to the surface.

Figure 3 shows scanning electron microscopy images of mefenamic acid crystals obtained from methanol and milled at cryogenic temperatures at different milling cycles ($n=1$, 3, …,9). It is noticeable from Fig. 3a-i to e-i that particle size reduces with increasing milling cycles from $n=1$ to $n=9$. SEM images at 6,000×

Fig. 2 Acid–base surface energy at three different fractional surface coverages (n/n_m) for mefenamic acid crystals milled at cryogenic temperature.
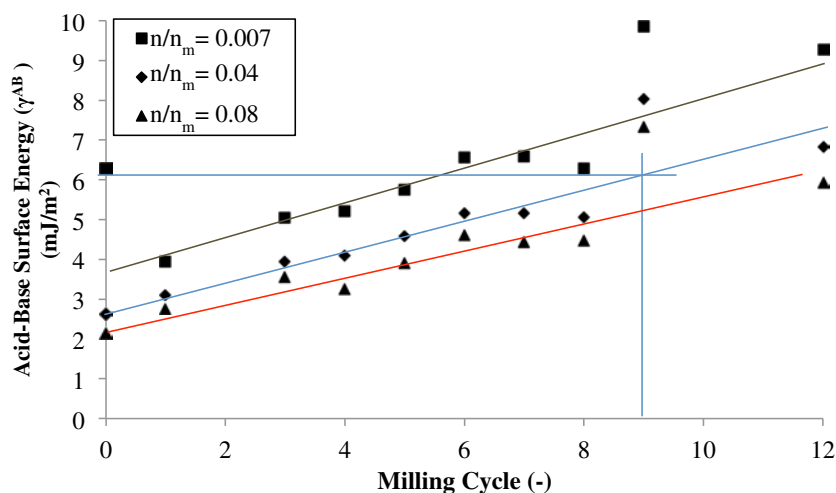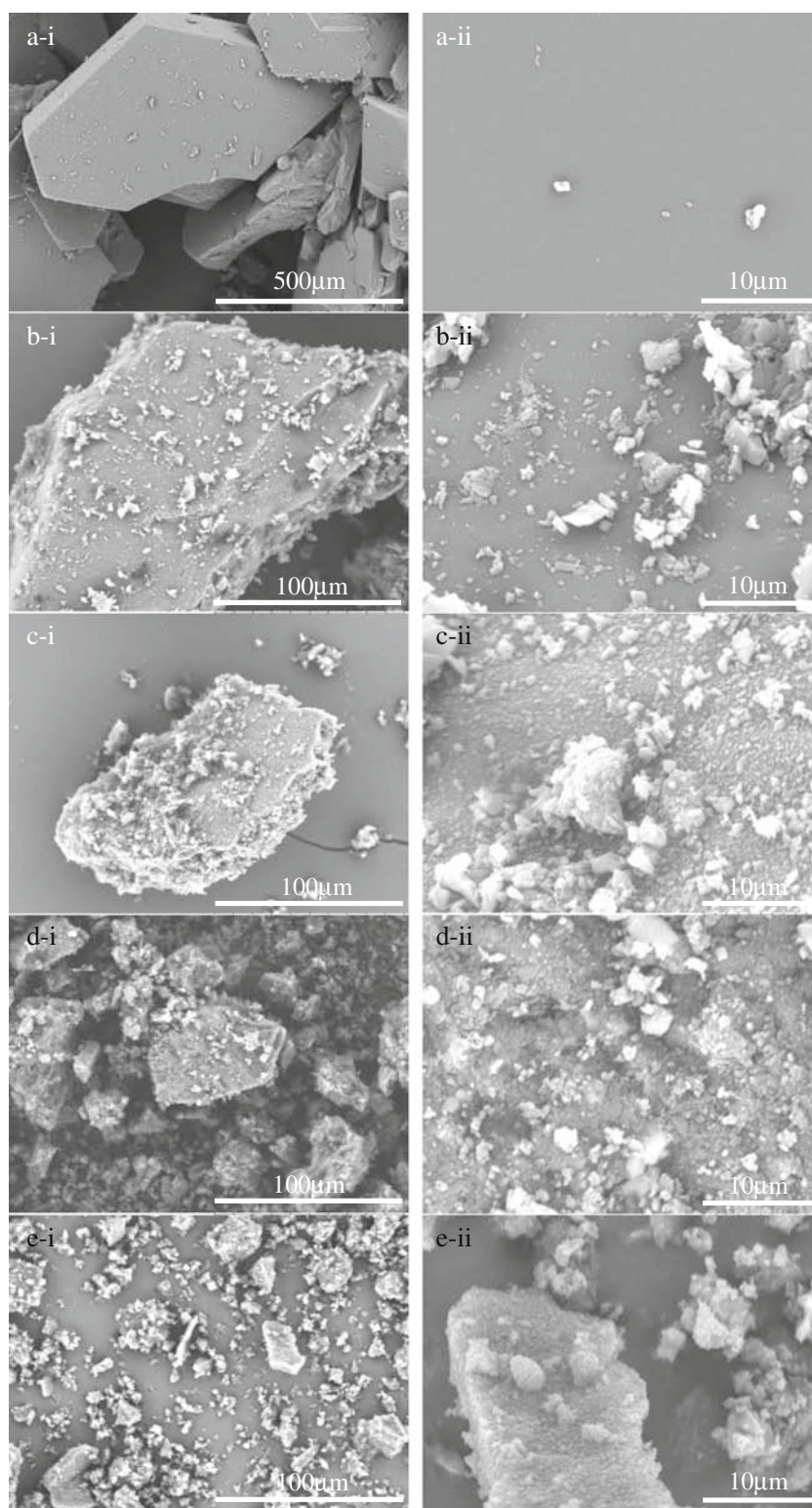
Fig. 3 Scanning Electron Microscopy (SEM) images of mefenamic acid (**a**) crystallised from methanol, (**b**) after cryogenic milling cycle-1, (**c**) after cryogenic milling cycle-3, (**d**) after cryogenic milling cycle-6, and (**e**) after cryogenic milling cycle-9. (Low resolution images are presented in (*x*-i) and that of high resolution in (*x*-ii)).

magnification were taken to visualise the effect of milling on the surface disorder or presence of fine particles (<1-2 μm) (which is postulated to be amorphous) on the particulate surface (Fig. 3a-ii to e-ii). Fig. 3a-i and a-ii show the un-milled mefenamic acid crystals obtained from methanol. It can be observed from Fig. 3a-ii that the crystal surface is very flat and has no disorder or negligible presence of very small particles (<1–2 μm). As milling cycle increases, an increase of very small particles (<1–2 μm) on the crystalline particulate surface can

Fig. 4 Effect of milling time on specific heat of transition and dispersive surface energy of mefenamic acid.
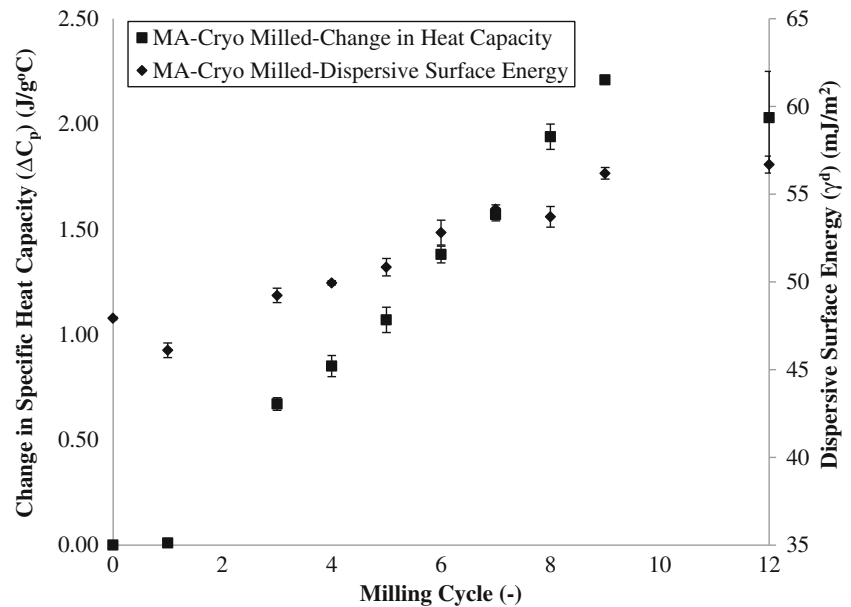
be observed from the Fig. 3b-ii to e-ii. Furthermore, SEM images obtained after milling cycle-9 (Fig. 3e-ii) suggested that crystalline particles are found to be covered with very small particles (<1 μm) agreeing with the initial hypothesis of surface saturation of amorphous particles Although SEM resolution may not be high enough to clearly show surface defects by milling, qualitatively SEM images demonstrate the changes in the particulate surface texture.

Impact of milling was postulated to result in generation of amorphous content on the particulate surface which was experimentally investigated using differential scanning calorimetry. Fig. 4 shows the change in specific heat of transition (ΔC_p), which is directly proportional to the amount of amorphous content present in the sample, (42) as a function of milling cycles. The secondary axis of Fig. 4 shows the dispersive component of the surface energy as a function of milling cycles. It is evident from Fig. 4 that with increasing milling cycles, the

amount of amorphous content detected in the milled sample increases as well.

Crystalline state has regular arrangement of its constituent molecules into fixed and rigid pattern known as lattice (43). It is well known that when crystalline particles are subjected to processing, the molecular order of crystalline material, particularly at the particle surface, is disrupted resulting in an amorphous phase. The amorphous form is a molecularly disordered form and hence is at a higher energy state. Considering this higher energy state of the amorphous form, it has been suggested that the amorphous forms possess higher surface energy compared to crystalline forms (44,45). From the discussion and experimental evidences provided in this study, the amount of surface amorphous content increases with increasing milling cycles, resulting in an increase in the surface energy.

The unconfined yield stress as a function of consolidation stress for mefenamic acid milled at different milling cycles

Fig. 5 Unconfined yield stress measured using uni-axial compression test for mefenamic acid crystals obtained from methanol and milled at cryogenic temperatures (surface area values in m²/g are shown in the bracket).
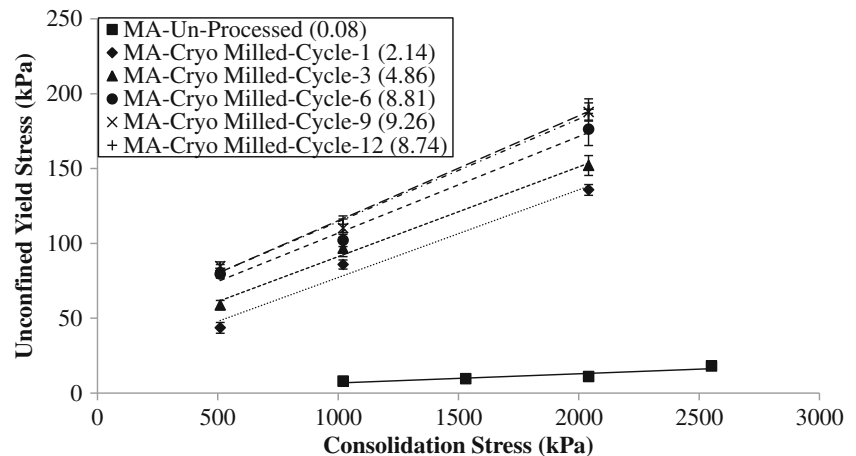
Table I Effect of Silanisation on Cohesion of Mefenamic Acid Crystals Obtained from Methanol and Milled at Cryogenic Temperature

Mefenamic acid crystals obtained from methanol	Cryogenic milling (Unsilanised)		Cryogenic milling (Silanised)	
	Cohesion (kPa)	Angle of internal friction (°)	Cohesion (kPa)	Angle of internal friction (°)
Un-processed	0.65	0.4	0.25	0.2
Milled-Cycle-1	18.65	3.4	10.27	1.3
Milled-Cycle-3	31.14	3.4	12.63	1.5
Milled-Cycle-6	42.30	3.9	17.80	1.6
Milled-Cycle-9	45.79	3.9	19.88	1.8
Milled-Cycle-12	44.97	4.0	20.01	1.9

($n=1, 3, \ldots, 12$) is shown in Fig. 5. The calculated cohesion and angle of internal friction values are shown in Table 1, suggesting that cohesion also increases with increasing milling cycles. This can be attributed to changes in three particle properties due to milling; particle size/surface area, particle shape, and surface energy. Particle size and shape analysis using Morphologi G3s revealed that the mean arithmetic (number weighted) aspect ratio, calculated by dividing the width by the length, of particles post milling does not change as a function of milling cycles and remains similar for all milling cycles. However, the particle size reduces and surface area increases from $2 \, \text{m}^2/\text{g}$ to $10 \, \text{m}^2/\text{g}$ as milling cycle increases from 1 to 12. Increase in cohesion of milled mefenamic acid particles with increasing milling cycle can be attributed to the combined effect of surface area and surface energy. Furthermore, it can be observed from Fig. 5 that un-processed (un-milled) mefenamic acid crystals obtained from methanol has very low yield stress compared to cryo milled

mefenamic acid. Surface area for un-processed (un-milled) mefenamic acid was an order of magnitude lower compared to that of cryo milled mefenamic acid after cycle-1. Very low surface area is postulated to be the cause of lower yield stress and lower cohesion for un-processed mefenamic acid.

Isolating the Effect of Surface Energy and Surface Area on Cohesion

Surfaces of silanised mefenamic acid were characterised using X-ray Photoelectron Spectroscopy, which confirms the presence of silane layer with methyl functional end group on the surface (Fig. 6). Fig. 6a shows high resolution XPS survey spectra before and after silanisation. Peak detected approximately at 102 eV in the XPS spectrum of silanised mefenamic acid, was assigned to Si2p. This peak was absent in the XPS spectrum of unsilanised mefenamic acid. Two different peaks centred at 102.05 eV and 102.85 eV can be fitted in the deconvoluted Si2p high resolution spectrum (Fig. 6b). The 102.05 eV peak can be assigned to Si-C, whereas the peak at 102.85 eV can be assigned to Si-O (46,47). Presence of Si-O, suggests that Si is covalently bonded to the hydroxyl groups present on the mefenamic acid surface. As dichlorodimethylsilane (($Cl)_2$-Si-($CH_3)_2$) is used as the silanisation agent, an equal area ratio of both the peaks Si-O and Si-C can be expected, to suggest that the silanisation is effective. Three different peaks centred at 531.99 eV, 532.57 eV and 533.64 eV can be fitted in high resolution spectrum of O1s which can be assigned to O-Si, O=C and OH-C (Fig. 6c) (46,47). The presence of O-Si detected in the high resolution O1s spectrum points to the presence of the silane layer. Reduction in the proportion of area ratio of OH-C, unaltered area proportions of O=C and detection

Fig. 6 X-ray Photoelectron Spectroscopy spectra for mefenamic acid (**a**) survey spectra before and after silanisation, high resolution (**b**) Si2p and (**c**) O1s spectra for silanised mefenamic acid.
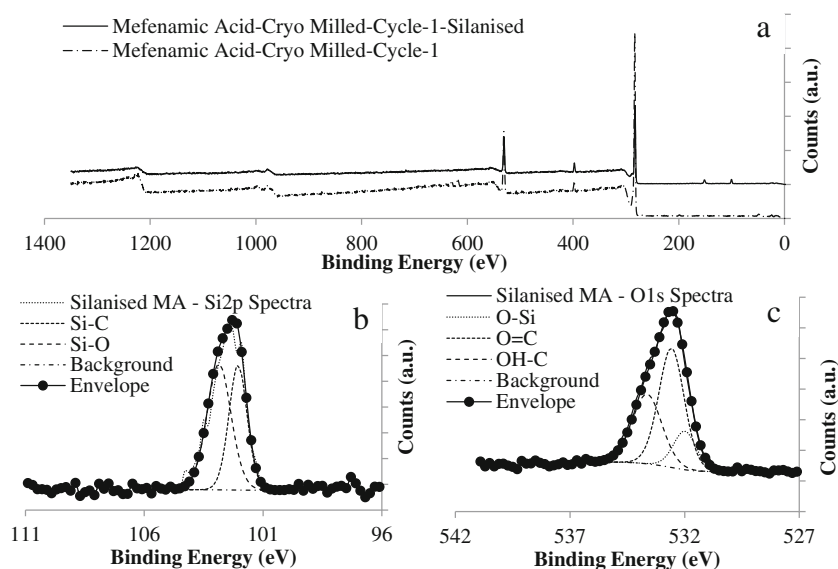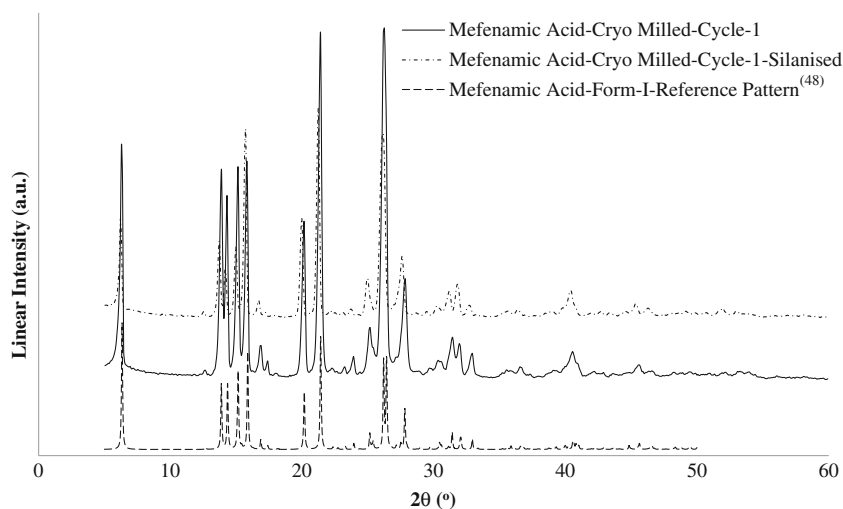
Fig. 7 Powder X-ray diffraction patterns of milled mefenamic acid powders before and after silanisation, compared with powder X-ray diffraction patterns reported for form-*I* mefenamic acid.

of peak with O-Si functionality post silanisation suggests surface is silanised. Findings of O1s spectrum are complementary to findings of Si2p. Furthermore, the analysis of C1s high resolution spectrum can be used to complement the findings of Si2p and O1s high resolution spectra, however considering molecular structure of mefenamic acid presence of C-O, C-C (aromatic), C-C, C-N, C=O can be observed in C1s spectrum. Additional detection of C-Si, post silanisation, can provide confirmation of silanisation from C1s spectra. C-C (aromatic) and C-Si has very close binding energies (284.7 eV for C-C (aromatic) and 284.3 eV for C-Si) and C-C (aromatic) has significantly higher presence in the spectra, considering that C-Si can only occur at the outer most molecular layer on the surface, it is very difficult to quantify presence of silane layer from C1s spectrum.

X-ray diffraction spectra were obtained before and after silanisation for mefenamic acid crystals milled at cryogenic milling temperature for one milling cycle to confirm that no polymorphic transformation has occurred during silanisation (Fig. 7). The X-ray diffraction spectra of silanised and un-silanised mefenamic acid were compared with the mefenamic acid polymorphic form-*I* powder diffraction spectra published in the literature (48). Both silanised and unsilanised mefenamic acid powders were identified to be the polymorphic form-*I*.

Effect of Surface Area on Cohesion

γ^d heterogeneity profiles for silanised and unsilanised cryomilled mefenamic acid samples are shown in Fig. 8. Surface energy was found to decrease with increasing fractional

Fig. 8 Effect of silanisation on dispersive component of surface energy of mefenamic acid milled at cryogenic temperatures.
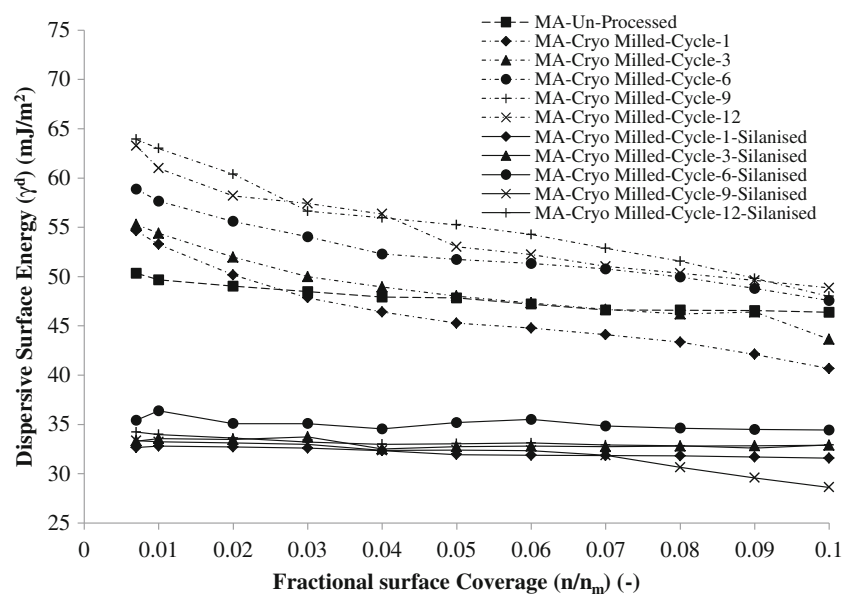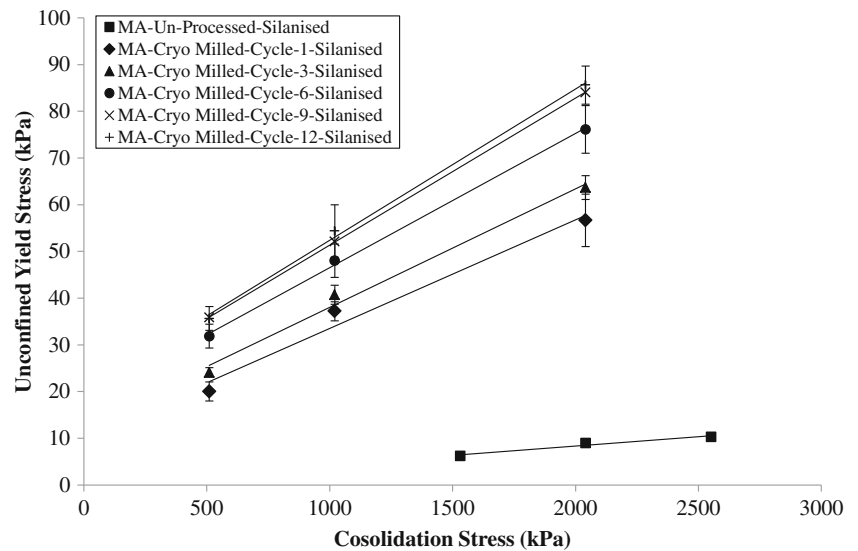
Fig. 9 Effect of silanisation on unconfined yield strength of mefenamic acid milled at cryogenic temperatures.

surface coverage for milled mefenamic acid samples. Such behaviour is not visible for the corresponding silanised samples, suggesting that the surface was energetically homogenous. For milling cycle-12, γ^d distributions displayed in Fig. 8, show that γ^d varied from 63.3 mJ/m^2 at 0.7% surface coverage to 48.9 mJ/m^2 at 10% surface coverage. For all silanised samples, γ^d remains relatively constant $(33.1 \pm 1.4$ mJ/m$^2)$. As a result of silanisation, the surface energy of the milled mefenamic acid material is found to be homogeneous and represents the coverage of particulate surface coverage with methyl functional end groups, which is in good agreement with the surface energy values published for the silanised surfaces with methyl functional end groups (16). Considering the homogeneous surface energy of post silanisation milled

mefenamic acid, the only variable affecting powder cohesion is the surface area.

Figure 9 shows unconfined yield stress measurements for silanised mefenamic acid. Comparing the sample prepared with a particular milling cycle/time and at a particular consolidation load, the yield stress is significantly lower for the silanised- mefenamic acid powders (Fig. 9) compared to the unsilanised powders (Fig. 5). The lower yield stress may be attributed to the reduction in the surface energy. Considering the thermodynamic work of cohesion, lower the surface energy lower the work of cohesion.

It can be observed from the Table 1 that cohesion for silanised mefenamic acid powders is lower compared to the unsilanised powders, however with increasing milling cycle/time cohesion

Fig. 10 Correlation of cohesion, measured using uni-axial compression test, as a function of surface area for silanised and unsilanised cryo milled mefenamic acid.
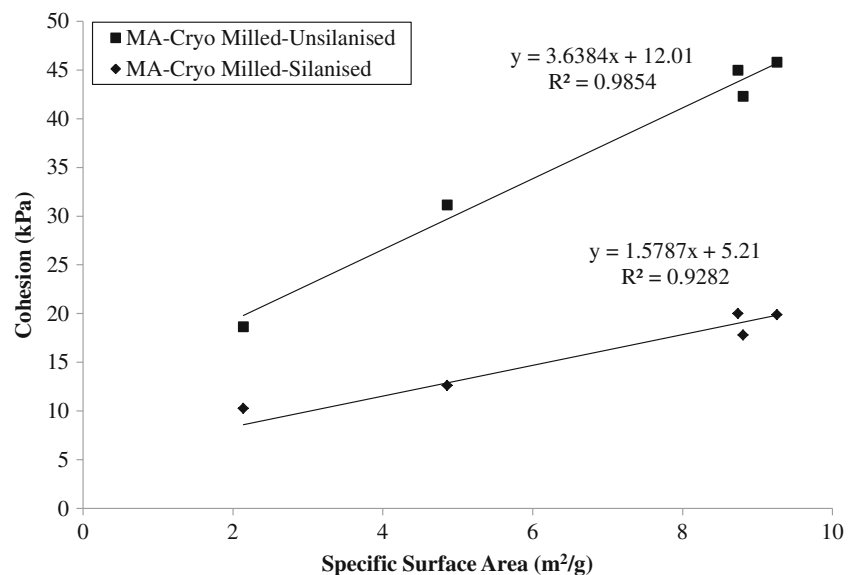
increase for unsilanised and silanised powders. Increase in the cohesion with increasing milling cycle for silanised samples can be attributed to the increase in surface area, as the surface energy for all silanised samples are similar and homogeneous.

Figure 10 shows a linear correlation between cryo milled mefenamic acid, which increases in surface area and surface energy, and powder cohesion. Post-milling silanisation of mefenamic acid further revealed the specific contribution of surface area to powder cohesion, which is minimal as discussed above. The contribution of surface energy can therefore be isolated by considering the surface area component of cohesion (silanised cryo milled mefenamic acid) as a ratio of the total cohesion (original cryo milled mefenamic acid). This is done by converging the ratio of gradients of best-fit lines of silanised and unsilanised cryo milled mefenamic acid, as well as that of the *y*-intercept of two best-fit lines to the same value, then dividing the gradient of silanised cryo milled mefenamic acid line by the gradient of original cryo milled mefenamic acid line. The remainder would be part of the surface energy contribution. For cryo milled mefenamic acid, the contribution from surface energy on cohesion was found to be ~57%, whereas contribution from surface area was quantified to be ~43%.

For the model system studied, the surface chemistry and surface area of the system apparently make approximately 57% and 43% contributions to the cohesion *i.e.* when surface chemistry is eliminated as a factor in cohesion, the remaining cohesion can readily be predicted from the surface area of the system. Such behaviour can be system specific as surface area and surface energy can be affected by the intrinsic properties of the material as well as processing parameters and observations made herein above can be different for each system and experimental conditions. However, the method reported in this study can be used to establish the contribution from surface area and surface energy on cohesion of pharmaceutical powders. Decoupling of the surface area and surface energy contribution will provide important information on which surface properties to control for controlling cohesion. Furthermore, an understanding of the role of particle processing methods on surface properties enables particle engineering with desired surface properties to control cohesion, *i.e.* the engineering of particle shapes, either by selecting processing solvents or by crystallisation conditions, will lead to particles with desired surface properties and ultimately improved powder handling.

CONCLUSIONS

This study demonstrates the effect of cryo-milling on the surface energy of mefenamic acid. Dispersive and acid base components of the surface energy were found to increase with increasing number of milling cycles, which was attributed to

surface amorphisation of mefenamic crystals. Powder cohesion was also found to increase with increasing milling time due to the increase in surface energy as well as surface area. An approach to decouple the contribution of surface area and surface energy by silanisation of powders is presented. Surface energy of powders was "normalised" by silanisation and hence, the cohesion of silanised powders can only be attributed to the contribution from surface area. For mefenamic acid, the contribution of surface area and surface energy to cohesion is found to be 43% and 57%, respectively. The decoupling approach presented in this study provides insight into the role of particle surface properties on powder cohesion.

ACKNOWLEDGMENT AND DISCLOSURES

REFERENCES

1. Fichtner F, Mahlin D, Welch K, Gaisford S, Alderborn G. Effect of surface energy on powder compactibility. Pharm Res. 2008;25(12): 2750–9.
2. Castellanos A. The relationship between attractive interparticle forces and bulk behaviour in dry and uncharged fine powders. Adv Phys. 2005;54(4):263–376.
3. Kumar A, Staedler T, Jiang X. Role of relative size of asperities and adhering particles on the adhesion force. J Colloid Interface Sci. 2013;409:211–8.
4. Podczeck F, Mia Y. The influence of particle size and shape on the angle of internal friction and the flow factor of unlubricated and lubricated powders. Int J Pharm. 1996;144(2):187–94.
5. Rasenack N, Müller BW. Crystal habit and tableting behavior. Int J Pharm. 2002;244(1–2):45–57.
6. Kaerger JS, Edge S, Price R. Influence of particle size and shape on flowability and compactibility of binary mixtures of paracetamol and microcrystalline cellulose. Eur J Pharm Sci. 2004;22(2–3):173–9.
7. Lam KK, Newton JM. Influence of particle size on the adhesion behaviour of powders, after application of an initial press-on force. Powder Technol. 1992;73(2):117–25.
8. Heng JYY, Bismarck A, Williams DR. Anisotropic surface chemistry of crystalline pharmaceutical solids. AAPS PharmSciTech. 2006;7(4): 12–20.
9. Planinšek O, Zadnik J, Kunaver M, Srčič S, Godec A. Structural evolution of indomethacin particles upon milling: time-resolved quantification and localization of disordered structure studied by IGC and DSC. J Pharm Sci. 2010;99(4):1968–81.
10. Smith AP, Shay JS, Spontak RJ, Balik CM, Ade H, Smith SD, *et al.* High-energy mechanical milling of poly (methyl methacrylate), polyisoprene and poly (ethylene-alt-propylene). Polym J. 2000;41(16):6271–83.
11. Wong LW, Pilpel N. The effect of particle shape on the mechanical properties of powders. Int J Pharm. 1990;59(2):145–54.
12. Farley R, Valentin FHH. Effect of particle size upon the strength of powders. Powder Technol. 1968;1(6):344–54.
13. Heng JYY, Williams DR. Wettability of paracetamol polymorphic forms I and II. Langmuir. 2006;22(16):6905–9.
14. Heng JYY, Bismarck A, Lee AF, Wilson K, Williams DR. Anisotropic surface chemistry of aspirin crystals. J Pharm Sci. 2007;96(8):2134–44.

15. Ho R, Heng JYY, Dilworth SE, Williams DR. Wetting behavior of ibuprofen racemate surfaces. J Adhes. 2008;84(6):483–501.
16. Ho R, Hinder SJ, Watts JF, Dilworth SE, Williams DR, Heng JYY. Determination of surface heterogeneity of d-mannitol by sessile drop contact angle and finite concentration inverse gas chromatography. Int J Pharm. 2010;387(1–2):79–86.
17. Heng JYY, Thielmann F, Williams DR. The effects of milling on the surface properties of form I paracetamol crystals. Pharm Res. 2006;23(8):1918–27.
18. Ho R, Naderi M, Heng JYY, Williams DR, Thielmann F, Bouza P, et al. Effect of milling on particle shape and surface energy heterogeneity of needle-shaped crystals. Pharm Res. 2012;29(10):2806–16.
19. Thielmann F, Burnett DJ, Heng JYY. Determination of the surface energy distributions of different processed lactose. Drug Dev Ind Pharm. 2007;33(11):1240–53.
20. Das SC, Stewart PJ. Characterising surface energy of pharmaceutical powders by inverse gas chromatography at finite dilution. J Pharm Pharmacol. 2012;64(9):1337–48.
21. Al-Chalabi SAM, Jones AR, Luckham PF. A simple method for improving the dispersability of micron-sized solid spheres. J Aerosol Sci. 1990;21(6):821–6.
22. Schultz J, Lavielle L, Martin C. The role of the interface in carbon fibre-epoxy composites. J Adhes. 1987;23(1):45–60.
23. Van Oss CJ, Chaudhury MK, Good RJ. Interfacial Lifshitz-van der Waals and polar interactions in macroscopic systems. Chem Rev. 1988;88(6):927–41.
24. Das SC, Larson I, Morton DAV, Stewart PJ. Determination of the polar and total surface energy distributions of particulates by inverse gas chromatography. Langmuir. 2010;27(2):521–3.
25. Fowkes FM. Determination of interfacial tensions, contact angles, and dispersion forces in surfaces by assuming additivity of intermolecular interactions in surfaces. J Phys Chem. 1962;66(2):382.
26. Owens DK, Wendt RC. Estimation of the surface free energy of polymers. J Appl Polym Sci. 1969;13(8):1741–7.
27. Etzler FM. Characterisation of surface free energies and surface chemistry of solids. In: Mittal KL, editor. Contact angle, wettability and adhesion. Utrecht, The Netherlands: VSP; 2003. p. 219–63.
28. Dorris GM, Gray DG. Adsorption of n-alkanes at zero surface coverage on cellulose paper and wood fibers. J Colloid Interface Sci. 1980;77(2):353–62.
29. Panzer U, Schreiber HP. On the evaluation of surface interactions by inverse gas chromatography. Macromolecules. 1992;25(14):3633–7.
30. Volpe CD, Siboni S. Some reflections on acid–base solid surface free energy theories. J Colloid Interface Sci. 1997;195(1):121–36.
31. Clint JH, Dunstan TS. Acid–base components of solid surfaces and the triboelectric series. Europhys Lett. 2001;54(3):320.
32. Ho R, Heng JYY. A review of inverse gas chromatography and its development as a tool to characterize anisotropic surface properties of pharmaceutical solids. Kona Powder Part J. 2013;30:164–80.
33. Gamble JF, Chiu WS, Tobyn MJ. Investigation into the impact of sub-populations of agglomerates on the particle size distribution and flow properties of conventional microcrystalline cellulose grades. Pharm Dev Technol. 2011;16(5):542–8.
34. Wang D. Advanced physical characterisation of milled pharmaceutical solids, PhD Thesis. London: Imperial College London; 2013.
35. Head KH. Manual of soil laboratory testing. 2nd ed. New York: Pantech Press; 1994.
36. Guoxian L, Erde W, Zhongren W. Effects of ball-milling intensity on the amorphization rate of mixed Ni50Ti50 powders. J Mater Process Technol. 1995;51(1–4):122–30.
37. Mackin L, Zanon R, Park JM, Foster K, Opalenik H, Demonte M. Quantification of low levels (<10%) of amorphous content in micronised active batches using dynamic vapour sorption and isothermal microcalorimetry. Int J Pharm. 2002;231(2):227–36.
38. Hüttenrauch R, Fricke S, Zielke P. Mechanical activation of pharmaceutical systems. Pharm Res. 1985;2(6):302–6.
39. Ksiażek K, Wacke S, Górecki T, Cz G. Effect of the milling conditions on the degree of amorphization of selenium by milling in a planetary ball mill. J Phys Conf Ser. 2007;79(1):012037.
40. Crowley KJ, Zografi G. Cryogenic grinding of indomethacin polymorphs and solvates: assessment of amorphous phase formation and amorphous phase physical stability. J Pharm Sci. 2002;91(2):492–507.
41. Elamin AA, Sebhatu T, Ahlneck C. The use of amorphous model substances to study mechanically activated materials in the solid state. Int J Pharm. 1995;119(1):25–36.
42. Hurtta M, Pitkänen I. Quantification of low levels of amorphous content in maltitol. Thermochim Acta. 2004;419(1–2):19–29.
43. Mullin JW. Crystallization. Oxford: Elsevier Butterworth-Heinemann; 2001.
44. Zhang J, Ebbens S, Chen X, Jin Z, Luk S, Madden C, et al. Determination of the surface free energy of crystalline and amorphous lactose by atomic force microscopy adhesion measurement. Pharm Res. 2006;23(2):401–7.
45. Ward S, Perkins M, Zhang J, Roberts CJ, Madden CE, Luk SY, et al. Identifying and mapping surface amorphous domains. Pharm Res. 2005;22(7):1195–202.
46. Briggs D, Seah MP. Practical surface analysis by ager and X-ray photoelectron spectroscopy. 1st ed. New York: Wiley; 1983.
47. Beamson G, Briggs D. High resolution XPS of organic polymers, the scienta ESCA300 database. 1st ed. Chichester: Wiley; 1992.
48. SeethaLekshmi S, Guru Row TN. Conformational polymorphism in a non-steroidal anti-inflammatory drug, mefenamic acid. Cryst Growth Des. 2012;12(8):4283–9.